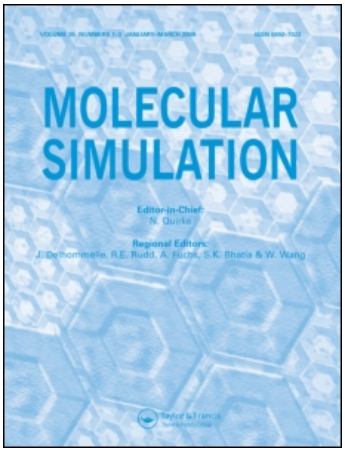


**Molecular Simulation**
Publication details, including instructions for authors and subscription information:
http://www.informaworld.com/smpp/title~content=t713644482

# A Comparison of Different Numerical Propagation Schemes for Solving the Time-Dependent Schrödinger Equation in the Position Representation in One Dimension for Mixed Quantum-and Molecular Dynamics Simulations

S. R. Billeter[a]; W. F. Van Gunsteren[a]
[a] Physical Chemistry, ETH Zentrum, Zürich, Switzerland

**To cite this Article** Billeter, S. R. and Van Gunsteren, W. F.(1995) 'A Comparison of Different Numerical Propagation Schemes for Solving the Time-Dependent Schrödinger Equation in the Position Representation in One Dimension for Mixed Quantum-and Molecular Dynamics Simulations', Molecular Simulation, 15: 5, 301 — 322
**To link to this Article: DOI:** 10.1080/08927029508022343
**URL:** http://dx.doi.org/10.1080/08927029508022343

*Molecular Simulation*, 1995, Vol. 15, pp. 301–322
Reprints available directly from the publisher
Photocopying permitted by license only



# A COMPARISON OF DIFFERENT NUMERICAL PROPAGATION SCHEMES FOR SOLVING THE TIME-DEPENDENT SCHRÖDINGER EQUATION IN THE POSITION REPRESENTATION IN ONE DIMENSION FOR MIXED QUANTUM- AND MOLECULAR DYNAMICS SIMULATIONS

S. R. BILLETER and W. F. VAN GUNSTEREN

*Physical Chemistry, ETH Zentrum, CH-8092 Zürich, Switzerland*

*(Received May 1995, accepted June 1995)*



Various numerical integration schemes to calculate the propagation of a state following the time-dependent Schrödinger equation in the one dimensional position representation are presented and compared to each other. Three potentials have been used: a harmonic, a double-well and a zero potential. Eigenstates and a coherent state have been chosen as initial states. Special attention has been given to the long-time stability of the algorithms. These are: kinetic referenced split operator (KRSO), kinetic referenced Cayley (KRC), distributed approximating functions (DAF), Chebysheff expansion (CH), residuum minimization (RES), second-order differencing (SOD), an eigenstate expansion (EE) and a corrected kinetic referenced split operator (CKRSO). In addition, a speedup of the KRC and KRSO methods is presented which is specially suited when very few grid points are used. Numerical results are compared to analytically calculated values. Mixed classical/quantum mechanical simulations require a representation of the quantum state on a limited number of grid points, classical integration time steps of about one femtosecond and compatibility with methods to solve the time-ordering problem. For the considered potentials which differ quite essentially from the potentials used for scattering problems in particle physics, the EE method has been found to be faster, more accurate and more stable than the other methods if only a few grid points are required. Otherwise, good results have been obtained with KRC, KRSO, CH, DAF and RES. SOD has been found to be too slow, and CKRSO is not stable enough for long simulation times.

KEY WORDS: Molecular dynamics, quantum dynamics, propagation, Schrödinger equation

## INTRODUCTION

With growing computer speed, molecular dynamics (MD) simulations with a subsystem that follows quantum mechanics (QM) become an interesting tool to study not only equilibrium properties but also reaction mechanisms [1]. There exist expressions to derive time-dependent properties from canonical ensembles using correlation functions and the golden rule [2–4], but one might prefer a direct insight into the time evolution of the system.

The problem of the time evolution of a given state function under the influence of an arbitrary Hamiltonian is not new: opticians have similar equations to solve when developing optical instruments; even Huygens' principle is such an old non-numeric

solution for light waves. The propagator (Green's function) is the operator $\hat{G}(t)$ which transforms an initial state function $|\Psi(0)\rangle$ into a state function at a later time:

$$|\Psi(t)\rangle = \hat{G}(t)|\Psi(0)\rangle. \tag{1}$$

Although time-dependent path integral simulations of chemical systems have only been performed in the near past, particle physicists have developed several methods to solve the time-dependent Schrödinger equation numerically using propagators. However, since the Hamiltonians of particle scattering problems and those of particles in liquid chemical systems differ quite essentially, it is not clear that the algorithms developed for particle scattering are useful, accurate and stable in mixed QM and classical-mechanical (CM) simulations. A formal solution of the Schrödinger equation

$$-\frac{\hbar}{i}\frac{\partial}{\partial t}|\Psi(t)\rangle = \hat{H}(t)|\Psi(t)\rangle \tag{2}$$

is

$$|\Psi(t)\rangle = \hat{T}\exp\left[-\frac{i}{\hbar}\int_0^t dt'\hat{H}(t')\right]|\Psi(0)\rangle, \tag{3}$$

which is of no practical use due to the time ordering operator $\hat{T}$. $\hat{H}(t')$ represents the Hamilton operator at time $t'$ and $\hbar$ is Planck's constant divided by $2\pi$. Several methods to circumvent this problem have been proposed: Magnus approximations [5], stationary formalisms using the Floquet theorem such as the $(t,t')$ method [6–8] and perturbation theory [9]. They all reduce the problem described by a time-dependent Hamiltonian to a problem with a time-independent Hamiltonian instead. It should be stated that Magnus approximations and stationary formalisms need an explicit time-dependence of the Hamiltonian, while perturbation theory uses values which are known at the beginning of the integration step to derive the correction terms. If the explicit time-dependence of the Hamiltonian is known, one might also consider dividing the integration time step into small substeps, each of them having its own constant Hamiltonian operator. However, it is difficult to apply these methods in mixed quantum-classical dynamics simulations, since the explicit time dependence is not known exactly. Whatever method is chosen to solve the time ordering problem, the need for propagation under the influence of a constant potential remains.

Assuming the Hamiltonian being time-independent during the interval $t$, the propagator is

$$|\Psi(t)\rangle = \exp\left(-\frac{i}{\hbar}\hat{H}t\right)|\Psi(0)\rangle. \tag{4}$$

Two problems arise from Eq. (4). First, the kinetic energy operator for a 1-dimensional particle with mass $m$

$$\hat{K} = -\frac{\hbar}{2m}\frac{\partial^2}{\partial x^2} \tag{5}$$

contained in the Hamiltonian $\hat{H} = \hat{K} + \hat{V}$ is non-local in the position representation, and second, the potential energy operator $\hat{V}$ and the kinetic energy operator $\hat{K}$ do not commute. The aim of this article is to present different ways to get around these problems and to compare them for their suitability to propagate one dimensional states in a molecular dynamics simulation. The particularities of such simulations are: relatively few grid points and smooth, time-dependent potentials whose time dependence is not explicitly known.

## METHODS

### *The Kinetic Referenced Split Operator and Cayley Techniques*

The Heisenberg uncertainty principle leads to

$$[\hat{K},\hat{V}] = \hat{K}\hat{V} - \hat{V}\hat{K} = -\frac{\hbar^2}{2m}\left[\left(\frac{\partial^2}{\partial x^2}V(\hat{x})\right) + 2\left(\frac{\partial}{\partial x}V(\hat{x})\right)\frac{\partial}{\partial x}\right], \tag{6}$$

where $\hat{x}$ is the position operator, and $[.,.]$ is the commutator. Under the condition

$$[\hat{K},[\hat{K},\hat{V}]] = [\hat{V},[\hat{K},\hat{V}]] = 0 \tag{7}$$

one would have

$$\exp\left(-\frac{i}{\hbar}\hat{H}t\right) = \exp\left(-\frac{i}{\hbar}\left(\hat{K}+\hat{V}\right)t\right) = \exp\left(-\frac{i}{\hbar}\hat{K}t\right)\exp\left(-\frac{i}{\hbar}\hat{V}t\right)\exp\left(\frac{i}{\hbar}\left[\hat{K},\hat{V}\right]\frac{t}{2}\right). \tag{8}$$

However, expression (6) does normally not commute with the kinetic energy operator, so condition (7) is not fulfilled. The simplest approximation (correct up to the first order in the commutator) to evaluate (8) would be to omit the exponential of the commutator in (8). However, the formulae

$$\exp\left(-\frac{i}{\hbar}\hat{H}t\right) \simeq \exp\left(-\frac{i}{\hbar}\frac{\hat{V}t}{2}\right)\exp\left(-\frac{i}{\hbar}\hat{K}t\right)\exp\left(-\frac{i}{\hbar}\frac{\hat{V}t}{2}\right) \tag{9}$$

$$\exp\left(-\frac{i}{\hbar}\hat{H}t\right) \simeq \left(1+\frac{i}{\hbar}\frac{\hat{V}t}{2}\right)^{-1}\exp\left(-\frac{i}{\hbar}\hat{K}t\right)\left(1-\frac{i}{\hbar}\frac{\hat{V}t}{2}\right) \tag{10}$$

which are correct up to the second order in the commutator do not require much additional computational expense. Eq. (9) is the kinetic referenced split operator (KRSO), and Eq. (10) is the kinetic referenced Cayley (KRC) formula [1, 10–12]. An advantage of these two product formulae is that $\hat{V}$ is diagonal in position space and $\hat{K}$ is diagonal in momentum space, allowing the use of Fast Fourier Transform (FFT) techniques for their evaluation. The upper limit of the integration time step is

determined by the size of the commutator and is usually much shorter than an integration time step required for a classical MD simulation. This makes the KRSO and KRC schemes relatively slow. If the state function can be represented by only few points on the spatial grid, the computational speed may be enhanced in the following way: The full propagator matrix is calculated for a time step. Then, multiplying the matrix $n$ times recursively by itself, a propagator for a $2^n$ times as long time step is obtained, $n$ being the number of recursions. These newly introduced methods will be called KRC_S and KRSO_S, respectively.

Another possibility to increase the integration time step is to reduce the error in the commutator from the second to the third order. Taylor expansion of the respective exponentials gives the deviation of KRSO from the correct exponential. The deviation of the KRC from the exact exponential is equal to that of the KRSO up to the third order; let $\hat{k}$, $\hat{v}$ be two arbitrary non-commuting operators, then we have up to the third order in the operators $\hat{k}$ and $\hat{v}$:

$$\exp(\hat{k}+\hat{v}) = \exp\left(\frac{\hat{v}}{2}\right)\exp(\hat{k})\exp\left(\frac{\hat{v}}{2}\right) - \frac{1}{12}\hat{v}\hat{k}\hat{k} + \frac{1}{6}\hat{k}\hat{v}\hat{k} + \frac{1}{24}\hat{v}\hat{v}\hat{k}$$

$$- \frac{1}{12}\hat{k}\hat{k}\hat{v} - \frac{1}{12}\hat{v}\hat{k}\hat{v} + \frac{1}{24}\hat{k}\hat{v}\hat{v}. \tag{11}$$

Setting $\hat{k} = -(i/\hbar)\hat{K}t$ and $\hat{v} = -(i/\hbar)\hat{V}t$, this formula is the basis for a corrected kinetic referenced split operator technique (CKRSO), newly introduced here. However, the method turns out to be unstable, and the gain in CPU time is nearly compensated by the time needed to calculate the additional terms.

*The Second-Order Differencing Technique*

One of the oldest integration schemes of the time-dependent Schrödinger equation is based on its series expansion [10–12]:

$$|\Psi(t)\rangle = |\Psi(-t)\rangle - 2\frac{i}{\hbar}\hat{H}t|\Psi(0)\rangle + O(t^3). \tag{12}$$

The series is expanded symmetrically around $|\Psi(0)\rangle$ for two reasons: the time evolution should be symmetric, and the second-order term in $t$ disappears. When applying the Hamiltonian, the FFT can be used again for the kinetic energy term. Since this method is correct up to second order in the time step, even if kinetic and potential energy would commute, the time step must be very small, even much smaller than the step used for KRSO and KRC. There exist higher-order differencing algorithms [11], but they will not be considered here. The results obtained with (12) are indicated by SOD.

*The distributed approximating functions technique*

It is easy to show that the propagator itself fulfills the Schrödinger Eq. (2)

$$i\hbar\frac{\partial}{\partial t}\hat{G}(t) = \hat{H}\hat{G}(t). \tag{13}$$

The initial condition for the propagator matrix $G(x, x', t)$ follows from Eq. (1)

$$G(x, x', 0) \equiv \langle x' | \hat{G}(0) | x \rangle = \delta(x - x'). \tag{14}$$

Starting from plane waves $\phi_p(x, t)$

$$\phi_p(x, 0) = \exp\left(\frac{i}{\hbar} px\right) \tag{15}$$

and using

$$\phi(x, t) = \exp\left[\frac{i}{\hbar}\left(p(x - x') - \left(\frac{p^2}{2m} + V_0\right)t\right)\right]\phi(x', 0) \tag{16}$$

as a special solution of the Schrödinger Eq. (2) for the constant potential $V_0$, and integrating over the momenta $p$ in

$$G(x, x', t) = \left(\frac{1}{2\pi\hbar}\right)^{1/2} \int dp \cdot \exp\left[\frac{i}{\hbar}\left(p(x - x') - \left(\frac{p^2}{2m} + V_0 t\right)\right)\right], \tag{17}$$

we obtain an analytical expression for the propagator matrix completely in terms of position coordinates

$$G(x, x', t) = \left(\frac{m}{2\pi i\hbar t}\right)^{1/2} \exp\left[-\frac{i}{\hbar}\left(-\frac{m}{2t}(x - x')^2 + V_0 t\right)\right]. \tag{18}$$

Formula (18) cannot be used for the integration of the Schrödinger equation on a spatial grid; the locality of the state is only due to phase cancellations when integrating (18). To avoid aliasing, the phase difference between two neighbouring grid points must be less than $\pi$:

$$k\Delta x < \pi, \tag{19}$$

otherwise an artefact at the spatial frequency $(2\pi - k\Delta x)/\Delta x$ is obtained, $\Delta x$ being the grid spacing, $k$ a spatial frequency,

$$\exp(ik\Delta x) = \exp(i(2\pi - k\Delta x))^*; \quad 2\pi - k\Delta x < \pi. \tag{20}$$

Because the frequencies of the kinetic energy part of (18) increase with decreasing time step while the frequencies of the potential energy part decrease under the same conditions, the aliasing condition (19) usually cannot be satisfied at any time step. Makri [13] proposed an expression similar to (18) where the contributions from momenta larger than a reasonably chosen cutoff momentum are filtered out. At larger distances, the absolute value of this propagator decays with $|1/(x - x')|$, while the absolute value of (18) remains one over the whole space.

The fast oscillations of (18) are mathematical artefacts coming from the nonphysical delta functions serving as basis of the position representation. That is the reason why in [14–17] Gauss-Hermite functions whose spatial extent is sufficiently small, were chosen as basis. A full derivation of the free propagator $\hat{F}(t)$, the propagator for a zero potential, can be found in [14, 15]. Here only an outline is presented. The first step is to fit the state $\Psi(x,0)$ to the approximating functions $\{a_j(x,0)\}$, $\{x_j\}$ being the grid points:

$$\Psi(x,0) \simeq \sum_j \Psi(x_j,0) a_j(x,0) \tag{21}$$

$$a_j(x,0) = a_0(x - x_j, 0) \tag{22}$$

$$a_j(x_k,0) \neq \delta_{jk} \tag{23}$$

Then, the propagator matrix element $F_{j'j}(t)$ from grid point $x_j$ to grid point $x_{j'}$ is approximated by the fitting functions:

$$F_{j'j} = \langle x_j | \hat{F}(t) | x_{j'} \rangle \simeq (\hat{F}(t) a_{j'}(x,0))|_{x=x_j} = a_{j'}(x,t)|_{x=x_j} = a_0(x_j - x_{j'}, t) \tag{24}$$

This means that for any given approximating function $a_0(x,0)$, we need only to know its time evolution. The next step is to find a suitable set of approximating functions. Define the fitting function as a Gauss-Hermite series of the degree $N_{\exp}$

$$a_0(x,0) = \frac{\Delta x}{2\sigma_0} \exp(-y^2) \sum_{n=0}^{N_{\exp}/2} \left(-\frac{1}{4}\right)^n \frac{1}{n!\sqrt{2\pi}} H_{2n}(y) \tag{25}$$

with $y$ set as $y^2(x,0) = x^2/2\sigma_0^2$. $H_n(x)$ is the $n$th Hermite polynomial, $\Delta x$ the grid spacing. Gauss-Hermitians are eigenfunctions of the Fourier transform and thus allow the greatest possible extent with the narrowest bandwidth of the propagator. These fitting functions can now be evolved in the time. Gaussians evolve following

$$\hat{F}(t) \exp\left(-\frac{x^2}{2\sigma_0^2}\right) = \frac{\sigma_0}{\sigma(t)} \exp\left(-\frac{x^2}{2\sigma^2(t)}\right) \tag{26}$$

$$\sigma^2(t) = \sigma_0^2 + \frac{i\hbar t}{m}. \tag{27}$$

This can be used for the propagation of Gauss-Hermitians

$$\hat{F}(t) H_n(y) \exp(-y^2) = \left(-\frac{d}{dy}\right)^n \hat{F}(t) \exp(-y^2) = \left(\frac{\sigma_0}{\sigma(t)}\right)^{n+1} H_n(y) \exp(-y^2) \tag{28}$$

$$y^2(x,t) = \frac{x^2}{2\sigma^2(t)}, \tag{29}$$

and finally for the approximating functions

$$\hat{F}(t)a_0(x,0) = a_0(x,t) = \frac{\Delta x}{2\sigma_0}\exp(-y^2)\sum_{n=0}^{N_{exp}/2}\left(-\frac{1}{4}\right)^n\left(\frac{\sigma_0}{\sigma(t)}\right)^{2n+1}\frac{1}{n!\sqrt{2\pi}}H_{2n}(y). \tag{30}$$

As the last step, (30) has to be integrated to obtain the free propagator matrix $F(x, x', t) = \langle x'|\hat{F}(t)|x\rangle$ in terms of position coordinates

$$F(x, x', t) = \frac{1}{\sigma_0}\cdot\exp\left[-\frac{(x-x')^2}{2\sigma^2(t)}\right]\cdot\sum_{n=0}^{N_{exp}/2}\left(-\frac{1}{4}\right)^n\left(\frac{\sigma_0}{\sigma(t)}\right)^{2n+1}\frac{1}{n!\sqrt{2\pi}}$$

$$\cdot H_{2n}\left(\frac{x-x'}{\sqrt{2}\sigma(t)}\right) \tag{31}$$

The propagator (31) can now be split into a Gaussian and a "shape polynomial" $S_{N_{exp}}$:

$$F(x, x', t) = \exp\left[-\frac{(x-x')^2}{2\sigma^2(t)}\right]\cdot S_{N_{exp}}(x-x', t) \tag{32}$$

$$S_{N_{exp}}(x, t) = \frac{1}{\sigma_0}\cdot\sum_{n=0}^{N_{exp}/2}\left(-\frac{1}{4}\right)^n\left(\frac{\sigma_0}{\sigma(t)}\right)^{2n+1}\frac{1}{n!\sqrt{2\pi}}\cdot H_{2n}\left(\frac{x}{\sqrt{2}\sigma(t)}\right). \tag{33}$$

The propagator (32) no longer becomes more oscillatory with decreasing time steps. The Gaussian envelope ensures numerical stability and fast convergence in Monte Carlo integration. Since this expression only contains position coordinates, the full propagator with a non-zero potential can be obtained by a simple multiplication

$$G(x, x', t) = F(x, x', t)\cdot\exp\left[-\frac{i}{\hbar}\frac{V(x)+V(x')}{2}\right]. \tag{34}$$

There exist other similar expressions. In the present work, only (34) was used. The results obtained with (34) are indicated by DAF.

*The Chebysheff Expansion Method*

Series expansions avoid the commutator problem in the in the exponential of Eq. (4). The Chebysheff expansion [10, 12] is not the only series expansion that has been successfully applied to propagation problems; the exponential Taylor series and a Lanczos series expansion [10, 12, 18] have been tested too. Since the Lanczos series has been compared to the Chebysheff series elsewhere [10], it is not described here.

The Chebysheff series expansion is well known for the range $\Omega_{re} = [-1, 1]$ with the weight function $w_{re}(x) = (1-x^2)^{1/2}$ and the scalar product $\langle f, g\rangle_{re} = \int_\Omega dx f^*(x)w_{re}(x)g(x)$ with $\Omega = \Omega_{re}$. The orthogonal basis functions $\{T'_n\}$ are then

proportional to the Chebysheff polynomials $\{T_n\}$

$$T'_0 = T_0/\sqrt{\pi} \tag{35}$$

$$T'_n(x) = T_n(x)\cdot\sqrt{2/\pi} \quad n > 0 \tag{36}$$

with the following recursion formulae:

$$T_0 = 1 \tag{37}$$

$$T_1(x) = x \tag{38}$$

$$T_{n+1}(x) = 2xT_n(x) - T_{n-1}(x). \tag{39}$$

For the purely imaginary Schrödinger equation we need a range $\Omega = [-i, i]$. Substituting $x$ by $\omega = ix$, we obtain the complex Chebysheff expansion

$$w(\omega) = (1 + \omega^2)^{1/2} \tag{40}$$

$$\phi_n(\omega) = i^n T_n(-i\omega) \tag{41}$$

$$\phi_0 = 1,\ \phi_1(\omega) = \omega,\ \phi_{n+1}(\omega) = 2\omega\phi_n(\omega) + \phi_{n-1}(\omega). \tag{42}$$

The Hamiltonian is normalized such that all its eigenvalues lie within $[-i, i]$:

$$\hat{H}_{\text{norm}} = 2\frac{\hat{H} - \hat{1}(\frac{1}{2}\Delta E + V_{\min})}{\Delta E} \tag{43}$$

$\Delta E$ is the energy range $V_{\max} + K_{\max} - V_{\min}$, and the maximum kinetic energy $K_{\max}$ is determined by the reciprocal grid spacing. The expression for the propagator is then

$$|\Psi(t)\rangle = \exp\left[-\frac{i}{\hbar}\left(\frac{1}{2}\Delta E + V_{\min}\right)t\right]\cdot\exp\left[-i\hat{H}_{\text{norm}}\cdot\frac{\Delta E t}{2\hbar}\right]\cdot|\Psi(0)\rangle. \tag{44}$$

Using the dimensionless phase space element $\alpha = \Delta E t/2\hbar$, the function $f(-i\hat{H}_{\text{norm}})$ is defined by

$$f(\omega) = f(-i\hat{H}_{\text{norm}}) = \exp\left[-i\hat{H}_{\text{norm}}\cdot\frac{\Delta E t}{2\hbar}\right] = \exp[-i\hat{H}_{\text{norm}}\cdot\alpha]. \tag{45}$$

With these definitions, the final expressions for the expansion (46), the coefficients (47) and the recursion (48) are:

$$|\Psi(t)\rangle \simeq \exp\left[-\frac{i}{\hbar}\left(\frac{1}{2}\Delta E + V_{\min}\right)t\right]\sum_{n=0}^{N_{exp}} a_n\left(\frac{\Delta E t}{2\hbar}\right)\phi_n(-i\hat{H}_{\text{norm}})\cdot|\Psi(0)\rangle \tag{46}$$

$$a_n(\alpha) = \frac{1}{\pi} C_n \cdot \langle \phi_n(-i\hat{H}_{\text{norm}}), \exp(-i\alpha\hat{H}_{\text{norm}}) \rangle = C_n \cdot J_n(\alpha),\ C_0 = 1,\ C_{n>0} = 2 \tag{47}$$

$$\Phi_{n+1}(-i\hat{H}_{\text{norm}}) = -2i\hat{H}_{\text{norm}}\Phi_n(-i\hat{H}_{\text{norm}}) + \Phi_{n-1}(-i\hat{H}_{\text{norm}});\ \Phi_0 = |\Psi(0)\rangle. \tag{48}$$

Note that the $\Phi_n$ are state functions, and only three of them have to be stored at one moment. The $J_n(\alpha)$ in the coefficients are the Bessel functions of the first kind and thus easy to calculate. The application of the normalized Hamiltonian is the most time-consuming step in this expansion. The FFT is applicable as well to save time. If the Hamiltonian varies only slowly, the series expansion can be done once for several simulation steps. The minimum degree of the expansion is limited by the dimensionless phase space element $\alpha = \Delta E t/2\hbar$, since the Bessel functions decay very rapidly when the argument is larger than the order. That is one reason for the high accuracy of this method. The results obtained here are indicated by CH.

*The Eigenfunction Expansion Method*

A very easy method to calculate the propagator is to expand the initial state in terms of the eigenfunctions of the Hamiltonian. Very powerful numerical routines are available for the diagonalization of matrices [19]. The expansion (49) is

$$|\Psi\rangle = \sum_n |n\rangle\langle n|\Psi\rangle, \tag{49}$$

and the propagation (50) is obtained when applying the propagation operator to the left side

$$\begin{aligned} |\Psi(t)\rangle = \sum_n |n\rangle\langle n|\Psi(t)\rangle &= \sum_n |n\rangle\langle n|\exp\left(-\frac{i}{\hbar}\hat{H}t\right)|\Psi(0)\rangle \\ &= \sum_n |n\rangle\left[\exp\left(-\frac{i}{\hbar}E_n t\right)\langle n|\Psi(0)\rangle\right]. \end{aligned} \tag{50}$$

$\{|n\rangle\}$ is a complete set of eigenstates of the Hamiltonian. Expression (50) has been used by Makri and coworkers for simulations in the quasi-adiabatic path integral approximation (QUAPI) [21, 22]. The computer resources required for a matrix diagonalization scales with about the third power of the matrix size. This means that this method is only applicable with very few grid points.

The Hamiltonian is represented by a real, symmetric matrix so that the QL decomposition can be applied after the calculation of a tridiagonal matrix [19]. Since usually higher excited states are almost unoccupied, one might consider an algorithm that calculates only a small fraction of the eigenstates. However, such algorithms need longer times per eigenfunction, and the number of eigenstates can also be reduced by the use of fewer grid points.

The Hamiltonian matrix can again be built using the FFT for the kinetic energy term. The operator $\hat{U}^{-1}\,\hat{K}\hat{U}$ is applied to the unity vectors to build the free Hamiltonian matrix, where $\hat{U}$ is the Fourier transform and $\hat{K}$ is the kinetic energy operator. This matrix remains the same throughout the simulation, and only the diagonal elements have to be recalculated every step from the potential. The results obtained with the eigenstate expansion are indicated by EE.

*The Residuum Minimization Method*

The residuum minimization method is a generalization of the Lanczos series expansion method [5, 18, 20]. Unlike in the EE method, not the whole range of the Hamiltonian is evaluated but only a Krylov subspace, spanned by $\{|\phi_i\rangle\}$

$$|\phi_i\rangle = \hat{H}^i|\Psi(0)\rangle. \tag{51}$$

The function $f(\hat{H}) = \exp[-(i/\hbar)t\hat{H}]$ can be expanded using a Newton polynomial series

$$f(\hat{H}) \simeq \sum_{n=0}^{N_{exp}} a_n P_n(\hat{H}), \tag{52}$$

$$P_0 = \hat{1},\ P_{n+1}(\hat{H}) = (\hat{H} - z_n\hat{1})P_n(\hat{H}) \tag{53}$$

with the interpolation points $\{z_n\}$. The expansion coefficients are the divided differences

$$a_0 = f(z_0),\quad a_1 = \frac{f(z_1) - a_0}{z_1 - z_0},\quad a_n = \frac{f(z_n) - \sum_{k=0}^{n-1} a_k P_k(z_k)}{P_n(z_n)}. \tag{54}$$

The idea is to choose the interpolation points $\{z_n\}$ such that the function $f(\hat{H})$ is interpolated by the Newton series as exactly as possible not over the whole range of the Hamiltonian but only over the part of interest, in this case the Krylov subspace (51). The points $\{z_n\}$ do not necessarily have to be chosen such that the function $f(\hat{H})$ is best expanded using $\{z_n\}$. In the residuum minimization method of [5, 20], the function $g(x) = 1/x$ has been chosen instead of $f(x) = \exp[-(i/\hbar)tx]$. The interpolation points are then the roots of the polynomial

$$R_{N_{exp}+1}(x) = \sum_{n=0}^{N_{exp}+1} c_n x^n, \tag{55}$$

$$b_i = \sum_{j=1}^{N_{exp}+1} S_{ij}c_j,\quad i = 1 \ldots N_{exp} + 1,\ c_0 = 1 \tag{56}$$

$$S_{ij} = \langle\phi_i|\phi_j\rangle,\quad b_i = -\langle\phi_i|\phi_0\rangle. \tag{57}$$

$[S_{ij}]$ is the overlap matrix of the Krylov vectors and $[b_j]$ is built from the overlap integrals of the initial state with the Krylov vectors. If the state and the Hamiltonian do not change essentially, the interpolation points do not have to be recalculated for each integration step. The Lanczos series expansion results from another choice of the function $g(x)$. The residuum minimization is not suited for high orders of expansion for two reasons: first, it needs additional stabilization and second, high orders of expansion increase basically the size of the Krylov subspace in which the error between the function $g(\hat{H})$ and the Newton series (52) is minimized and thus do not increase the maximum time step considerably, while the Chebysheff expansion is global (it can be applied over the whole range of the Hamiltonian) and higher orders of expansion mean a larger energy-time phase space element and thus allow for a longer time step. The residuum minimization using $g(x) = 1/x$ has been found to be somewhat superior to the Lanczos series [5]. The results obtained using the residuum minimization method are indicated by RES.

## MODELS



A one-dimensional particle with the mass of a proton $m_p = 1.008$ u was propagated in a zero potential, in a harmonic potential with the period $T_p = 10$ fs for the mass $m_p$ and in a double well potential of the form

$$V(x) = V_0 + V_m[(x - x_0)^{-12} + (x + x_0)^{-12} - (x - x_0)^{-6} - (x + x_0)^{-6}]. \tag{58}$$

with $V_0 = 285.8\,\text{kJ/mol}$, $V_m = 1270.2\,\text{kJ/mol}$ and $x_0 = 0.3\,\text{nm}$. Energy is measured in units $\hbar \cdot \text{ps}^{-1}$. As initial states we chose the ground state, the first and tenth excited state, the coherent state of the harmonic potential with initial elongation $< x_0 > = 0.001$ nm and the ground state of the double-well potential. The double well potential has a nonvanishing third derivative and a non-monotonic first derivative. It was chosen to test the capability of the integration methods to deal with such potentials too. The reason for the choice of the eigenstates was the availability of analytical solutions. The coherent state has been chosen because it is not time-independent while there is an analytical solution as well. In addition, a delta peak has been used as initial state to compare the numerically calculated free propagator to an analytically calculated expression.

The number of QM integration time steps per classical MD time step $N_{QM}$ and the number of grid points $N_P$ are adjustable parameters for all methods, while the degree of expansion $N_{\text{exp}}$ is a specific parameter of the CH, the DAF and the RES methods. The DAF propagation needs the initial extent of the Gaussian $\sigma_0$ as second specific parameter. The choice of these method-specific parameters is not difficult since inappropriate values yield completely wrong results. For numerical reasons, the accuracy cannot arbitrarily be increased as can be seen from Tables 1 and 2. Here, the ranges of $N_{QM}$ and, if required, $N_{\text{exp}}$ have been chosen such that $N_{QM}$ of the optimum accuracy of a method is covered by the range, but with one exception: the optimum $N_{QM}$ for SOD would need unreasonably long simulation times. For the choice of the

**Table 1** Accuracy as function of the number $N_{QM}$ QM integration time steps per CM time step. The ground state of the harmonic oscillator with a period of 10 fs and mass 1.008 u was propagated under the influence of the harmonic potential over 40 CM simulation steps of 2.5 fs. $\sigma(E_{kin})$ is the standard deviation of the kinetic energy from the average. The number of points $N_P$ on the grid was 32. Methods: kinetic referenced Cayley (KRC), kinetic referenced split operator (KRSO) and distributed approximating functions (DAF) with $N_{exp} = 100$ and the $\sigma_0 = 0.02$ nm

| $N_{QM}$ | $\sigma(E_{kin})[10^{-4}$ kJ/mol] | | |
|---|---|---|---|
| | *KRC* | *KRSO* | *DAF* |
| 64 | 3.271 | 7.556 | 7.513 |
| 128 | 0.843 | 1.917 | 1.884 |
| 256 | 0.400 | 0.312 | 0.485 |
| 512 | 0.167 | 0.330 | 0.151 |
| 1024 | 0.179 | 0.185 | 0.102 |
| 2048 | 0.401 | 0.915 | 0.138 |

**Table 2** Accuracy as function of the number $N_{QM}$ QM integration time steps per CM time step. $\sigma(E_{kin})$ is the standard deviation of the kinetic energy from the average in $10^{-4}$ kJ/mol. Methods: second order differencing (SOD), corrected kinetic referenced split operator (CKRSO), Chebysheff series expansion (CH) with the degree $N_{exp} = 30$ and residuum minimization (RES) with the degree $N_{exp} = 3$. Otherwise as in Table 1

| *SOD* | | *CKRSO* | | *CH* | | *RES* | |
|---|---|---|---|---|---|---|---|
| $N_{QM}$ | $\sigma(E_{kin})$ | $N_{QM}$ | $\sigma(E_{kin})$ | $N_{QM}$ | $\sigma(E_{kin})$ | $N_{QM}$ | $\sigma(E_{kin})$ |
| 4096 | 13.526 | 16 | 35.734 | 3 | 0.745 | 16 | – |
| 8192 | 6.762 | 32 | 4.458 | 6 | 0.015 | 32 | 0.005 |
| 16384 | 3.381 | 64 | 0.524 | 9 | 0.107 | 64 | 0.001 |
| 65536 | 0.846 | 128 | 0.080 | 12 | 0.202 | 128 | 0.002 |
| 131072 | 0.423 | 256 | 0.089 | | | 256 | 0.003 |
| 262144 | 2.212 | 512 | 0.259 | | | | |



degree of the RES expansion $N_{exp}$, we refer to [5]. Table 3 gives an overview over the performed calculations, and Table 4 lists the parameters.

## RESULTS

### *Overview, Time-Dependent Hamiltonians*

Table 5 shows how the CPU time and the storage requirements scale with the number of grid points ($N_P$), the typical number of QM integration steps ($N_{QM}$) within a classical time step of 2.5 fs and the degree of the series expansion ($N_{exp}$), if required. The DAF approach was developed to obtain an expression containing a Gaussian which makes this method specially suited for Monte Carlo simulations instead of MD-like schemes.

Since the split operator propagators (KRC, KRSO) are short-time expressions, they are specially suited for interpolated Hamiltonians which are assumed to be constant in

**Table 3** Overview over the simulations performed. For benchmark purposes, the Hellmann-Feynman forces to a hypothetical classical (CM) subsystem were calculated together with the potential energy part of the propagator

| *Run* | *time step* [$fs$] (CM) | *number of steps* (CM) | *potential* | *Hellmann-Feynman* |
|---|---|---|---|---|
| 1 | 15 | 1 | free | no |
| 2 | 15 | 5 | free | no |
| 3 | 2.5 | 40 | harmonic | no |
| 4 | 2.5 | 4000 | harmonic | no |
| 5 | 2.5 | 40 | harmonic | yes |
| 6 | 2.5 | 4000 | double-well | no |

**Table 4** Simulation parameters for the various integration methods. $N_P$: number of grid points, $N_{QM}$: number of QM integration time steps per classical time step, $N_{exp}$: degree of the series expansion, if required. ST stands for the analytical expression of the propagator in the position representation. For the other abbreviations, see the "Methods" section

| *Method* | $N_P$ | $N_{QM}$ | $N_{exp}$ |
|---|---|---|---|
| (ST) | 16, 32, 64 | 1 | – |
| KRC | 16, 32, 64 | 64, 256, 1024 | – |
| KRC_S | 16, 32, 64 | $2^6$, $2^8$, $2^{10}$ | – |
| KRSO | 16, 32, 64 | 64, 256, 1024 | – |
| KRSO_S | 16, 32, 64 | $2^6$, $2^8$, $2^{10}$ | – |
| CKRSO | 16, 32, 64 | 16, 32, 64, 128 | – |
| DAF, free | 16, 32, 64 | 64, 80, 100 | 100, 150, 200 |
| DAF, bound | 16, 32, 64 | 512, 640, 800 | 100, 150, 200 |
| CH, free | 16, 32, 64 | 1 | 20, 25, 30, 35 |
| CH, bound | 16, 32, 64 | 6 | 20, 25, 30, 35 |
| SOD | 16, 32, 64 | 4096, 16384 | – |
| EE | 16, 32, 64 | 1 | – |
| RES | 16, 32, 64 | 32, 64, 128, 256 | 2, 3, 5 |

**Table 5** Scaling properties of the different propagation algorithms. For the abbreviations, see Table 4

| *Method* | *limiting function* ($N_P \to \infty$) | *CPU time* | *storage* | $N_{QM}/N_{exp}$ |
|---|---|---|---|---|
| *(ST)* | *multiplication by a matrix* | $N_P^2$ | $4N_P$ | – |
| KRC | FFT | $N_P \ln N_P$ | $5N_P$ | large/1 |
| KRC_S | matrix multiplication | $N_P^3$ | $2N_P^2$ | 1/1 |
| KRSO | FFT | $N_P \ln N_P$ | $4N_P$ | large/1 |
| KRSO_S | matrix multiplication | $N_P^3$ | $2N_P^2$ | 1/1 |
| CKRSO | FFT | $N_P \ln N_P$ | $6N_P$ | medium/1 |
| DAF | multiplication by a matrix | $N_P^2$ | $4N_P$ | small/medium |
| CH | FFT | $N_P \ln N_P$ | $6N_P$ | small/medium |
| SOD | FFT | $N_P \ln N_P$ | $4N_P$ | very large/1 |
| EE | diagonalization of a matrix | $N_P^3$ | $2N_P^2$ | 1/1 |
| RES | FFT | $N_P \ln N_P$ | $4N_P$ | medium/small |

each short substep. This applies for the propagators obtained with the second-order differencing scheme (SOD) and the low-order iterative series expansions such as the Lanczos and residuum minimization series (RES) as well. Magnus approximations [5] can improve the result. The Chebysheff expansion (CH) has successfully been combined with the $(t, t')$ method [6], while the Lanczos and residuum minimization series (RES) have successfully been combined with Magnus approximations of the first and second order [5]. In principle, every global propagator (KRC_S, KRSO_S, DAF, CH, EE) can be combined with either Magnus approximations or stationary formalisms. The eigenstate expansion (EE) provides all eigenstates of the Hamiltonian and their expansion coefficients which both can be used for a perturbation theory correction for the time-dependent Hamiltonian so that its explicit time-dependence has not to be known. In addition, the energy eigenvalues and eigenstates can be used for an extended Hellmann-Feynman theorem for non-stationary states [9].

*Free Propagation: Choice of Parameters*

Figures 1 and 2 show how fast oscillations of a propagator can be replaced by a Gaussian decay of the envelope. These figures have been calculated directly using the corresponding formulae (18) and (31) in the "Methods" section. For the DAF method, we note the strong effect of the choice of the value of $\sigma_0$. Figure 3 shows a consequence



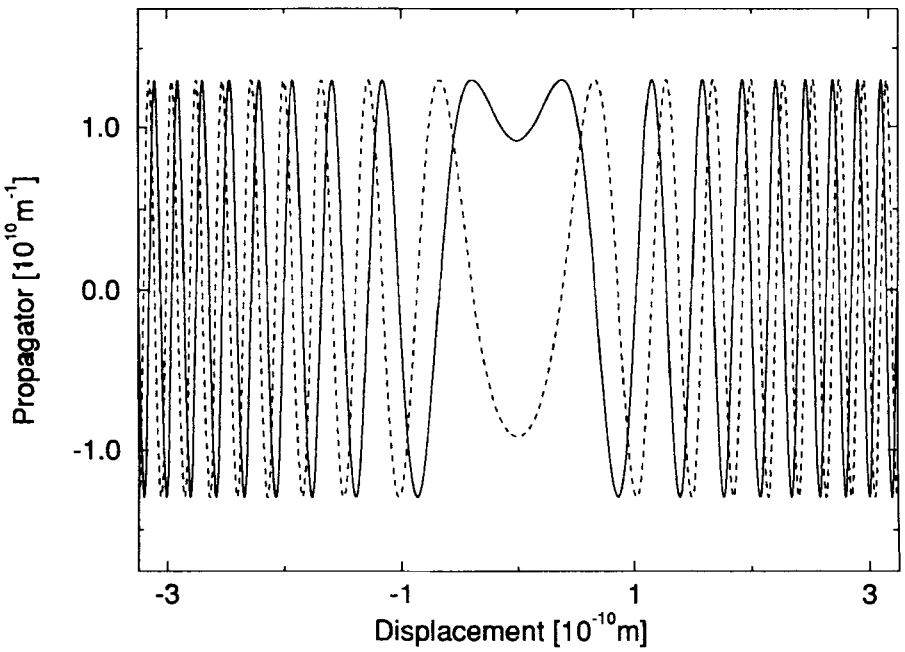


**Figure 1** The propagator matrix element $G(x, x', t)$ of a free particle ($V_0 = 0$) with mass 1.008 u, calculated using Eq. (18) for $t = 15$ fs as a function of the displacement $(x - x')$. The lines are the real part (solid line) and the imaginary part (dashed line).

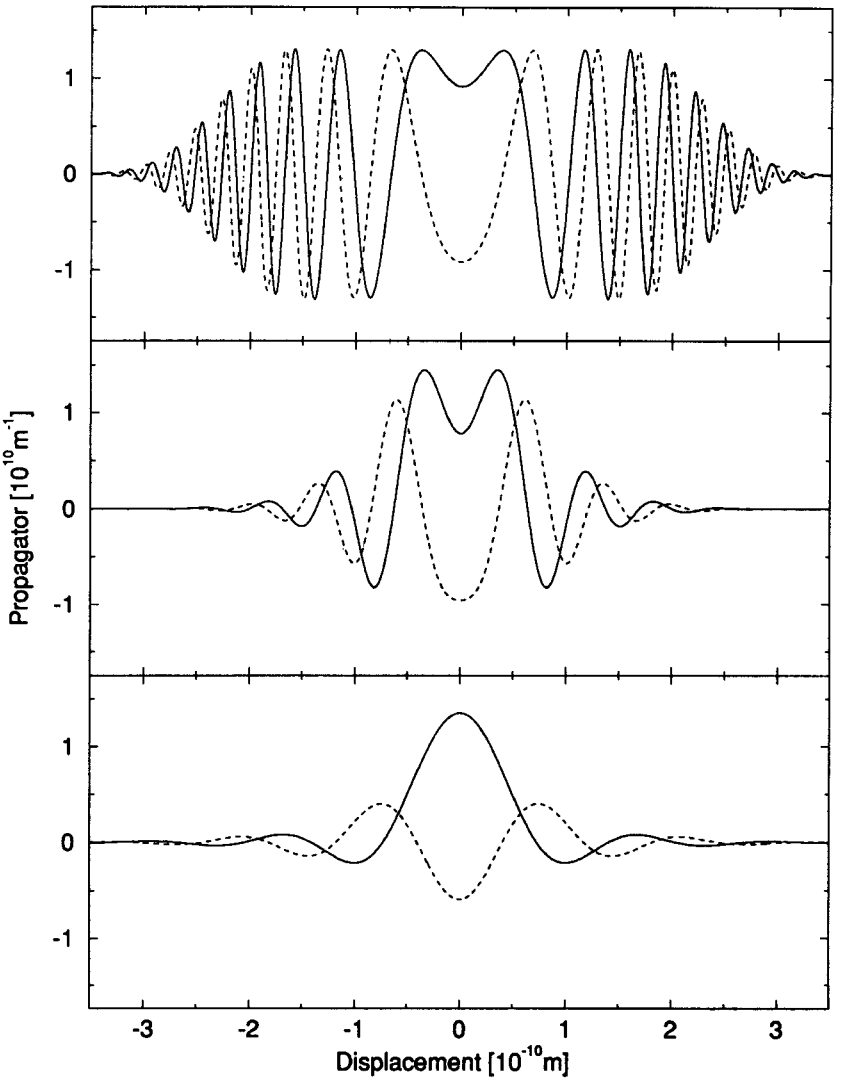


**Figure 2** The DAF propagator matrix element $F(x, x', t)$ of a free particle with mass 1.008 u, calculated using Eq. (31) for $t = 15$ fs as a function of the displacement $(x - x')$. The lines are the real part (solid line) and the imaginary part (dashed line). Top: $\sigma_0 = 0.02$ nm, middle: $\sigma_0 = 0.05$ nm, bottom: $\sigma_0 = 0.1$ nm.

of an improper choice of $\sigma_0$ when applying the free propagator to the ground state of a harmonic oscillator: The correct final state can be reproduced if the DAFs are chosen small enough with $\sigma_0 = 0.02$ nm, while $\sigma_0 = 0.05$ nm and $\sigma_0 = 0.1$ nm lead to wrong final states.

Figure 4 shows a convergence test of a complex Chebysheff series expansion of the function $\exp(-i \cdot \alpha \cdot x)$ in terms of $-i \cdot x$. It is clearly visible that convergence is reached very quickly as soon as the degree of the expansion, $N_{exp}$, is a larger number than

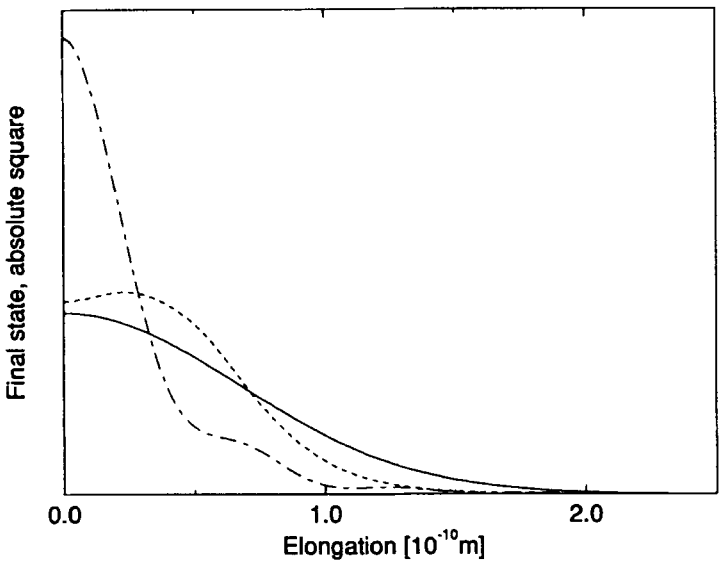


**Figure 3** Probability density of a final state resulting from free DAF propagation ($V_0 = 0$) of a particle with mass 1.008 u starting from the ground state of a harmonic potential with period 10 fs for $t = 15$ fs. The lines are from both the analytical solution Eq. (18) and DAF (Eq. (31)) with $\sigma_0 = 0.02$ nm (solid line), $\sigma_0 = 0.05$ nm (dashed line), $\sigma_0 = 0.1$ nm (dot-dashed line).



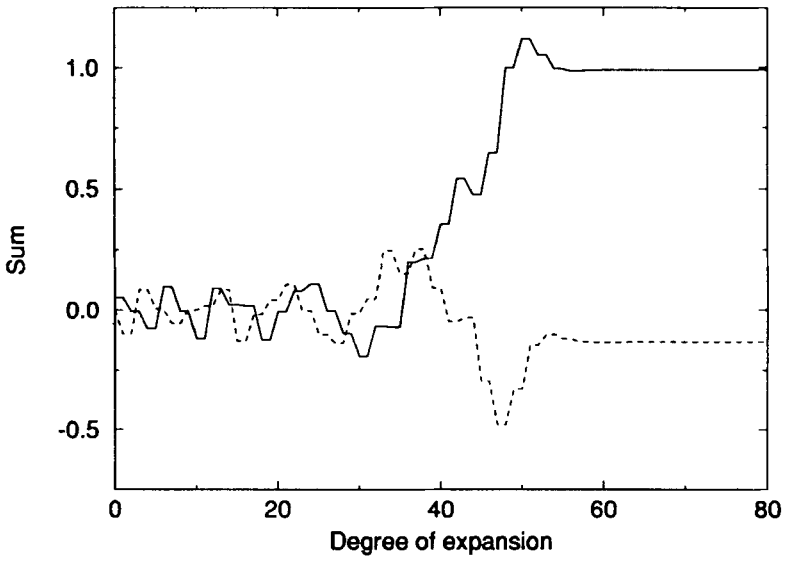


**Figure 4** A Chebysheff expansion of the imaginary function $f(x) = \exp(-i \cdot \alpha \cdot x)$ with $\alpha = 50$, $x = 0.5$, so $f(x) = 0.9912 - 0.1324i$, in terms of $-i \cdot x$ as a function of the degree ($N_{exp}$) of the expansion.

$\alpha$ which corresponds to the dimensionless phase space element in the Chebysheff expansion of the propagator.

*Full Propagation: Accuracy, Stability and Benchmarks*

The tables belonging to this section list only the results of the simulation that gives the best results in terms of the indicated quantity to be optimized for each method. Table 6 contains the results of simulations in vacuo of a particle in a harmonic oscillator in the ground state using 40 classical MD time steps of 2.5 fs. The expectation value for the kinetic energy is $(1/4)\hbar\omega = 9.97578$ kJ/mol. For each method, the values for the parameters $N_P$, $N_{QM}$, and $N_{\exp}$ which give the smallest standard deviation of the kinetic energy from the average, were selected from the parameter values given in Table 4. Use of more grid points $N_P$ does not necessarily imply better results, and so does the use of more QM time steps $N_{QM}$ per classical time step. Note that the standard deviation of the kinetic energy in the SOD simulation is still about 1/30000 of the kinetic energy. Table 7 contains the same quantities for 4000 instead of 40 simulation steps. The DAF and SOD methods produce almost the same error over 40 steps as over 4000 steps, while the errors of CKRSO increase by two orders of magnitude. Primarily, an integration scheme needs to be stable, so it is much more important that a method produces a nearly constant error over long times than an error which is initially small but increases with longer simulation times. One might consider the possibility to compensate a systematic drift in the kinetic energy by a coupling to a reference value, just as the kinetic energy can be kept stable over long classical MD simulations using weak coupling to a reference temperature [23].

It is known that the CH method allows for extremely high degrees of expansion and thus can solve a scattering problem over some picoseconds within one single integration step. In mixed quantum-classical dynamics simulation we cannot use this advan-



**Table 6** Accuracy of the various methods: Propagation of the ground state in a harmonic oscillator potential over 40 CM time steps of 2.5 fs. $E_{kin}$ is the kinetic energy, $\sigma(E_{kin})$ is its standard deviation from the average and $\sigma(norm)$ is the standard deviation of the norm of the state. $N_P$ is the number of grid points, $N_{QM}$ is the number of QM integration steps per classical MD step. The values of $N_P$, $N_{QM}$ and $N_{\exp}$ were selected from all combinations given in Table 4 such that the standard deviation of the kinetic energy $\sigma(E_{kin})$ from the average is minimal for each method. The asterisk indicates that the norm of the state is artificially kept at one in the DAF method. The rankings are derived from the standard deviation of the kinetic energy from the average. The potential energy behaves in the same manner as the kinetic energy. For the other abbreviations, see Table 4

| *Method* | *ranking* | $N_P$ | $N_{QM}/N_{exp}$ | $E_{kin}$ [kJ/mol] | $\sigma(E_{kin})[10^{-4}$kJ/mol] | $\sigma(norm)[10^{-4}]$ |
|---|---|---|---|---|---|---|
| KRC | 6 | 64 | 256/– | 9.9757573 | 0.126 | 0.003 |
| KRC_S | 8 | 64 | $2^8$/– | 9.9758549 | 2.202 | 0.069 |
| KRSO | 7 | 64 | 1024/– | 9.9757684 | 0.216 | 0.008 |
| KRSO_S | 9 | 32 | $2^8$/– | 9.9753154 | 2.372 | 0.118 |
| CKRSO | 5 | 32 | 128/– | 9.9757669 | 0.080 | 0.003 |
| DAF | 4 | 32 | 800/150 | 9.9757727 | 0.047 | 0.000* |
| CH | 1/2/3 | 32 | 1/150 | 9.9757774 | 0.002 | 0.000 |
| SOD | 10 | 16 | 16384/– | 9.9757774 | 3.381 | 0.169 |
| EE | 1/2/3 | 32 | 1/– | 9.9757774 | 0.002 | 0.000 |
| RES | 1/2/3 | 32 | 128/3 | 9.9757775 | 0.002 | 0.000 |

**Table 7** Numerical stability of the various methods: propagation of the ground state in a harmonic oscillator potential over 4000 CM time steps of 2.5 fs. Otherwise as in Table 6

| *Method* | *ranking* | $N_P$ | $N_{QM}/N_{exp}$ | $E_{kin}$ [kJ/mol] | $\sigma(E_{kin})[10^{-4}$kJ/mol] | $\sigma(norm)[10^{-4}]$ |
|---|---|---|---|---|---|---|
| KRC | 6 | 64 | 256– | 9.9756855 | 0.875 | 0.029 |
| KRC_S | 10 | 16 | $2^6$/– | 9.9796748 | 41.905 | 1.875 |
| KRSO | 5 | 64 | 256/– | 9.9758228 | 0.778 | 0.029 |
| KRSO_S | 9 | 32 | $2^6$/– | 9.9753923 | 7.781 | 0.105 |
| CKRSO | 8 | 16 | 128/– | 9.9746337 | 6.741 | 0.336 |
| DAF | 4 | 32 | 800/150 | 9.9757727 | 0.046 | 0.000* |
| CH | 3 | 32 | 1/210 | 9.9757762 | 0.030 | 0.001 |
| SOD | 7 | 32 | 16384/– | 9.9757775 | 3.382 | 0.169 |
| EE | 1 | 16 | 1/– | 9.9757774 | 0.007 | 0.000 |
| RES | 2 | 32 | 128/5 | 9.9757773 | 0.011 | 0.001 |

tage due to the classical MD step the size of which is usually around a femtosecond. A method does not only have to be accurate and stable, it also must be computationally fast. Table 8 shows the ranking of the methods with respect to the product of the user CPU time on a SUN Sparc 10 and the standard deviation of the kinetic energy. Tables 9 and 10 give a summary of the ranking of the methods when propagating the ground state, the first and tenth excited state of the harmonic oscillator and the ground state of the double-well potential. It is no surprise that the RES method breaks for the tenth excited state since the maximum degree of expansion was chosen to be 5 and thus the Krylov subspace is much too small to cover the tenth excited state. The eigenfunction expansion method seems to be the fastest and most accurate integration scheme for the propagation under the given conditions, but so far, all considered initial states have been eigenstates of the respective Hamiltonians. That is why a coherent state was chosen as an initial state as well. Table 11 shows the results of these simulations. Since



**Table 8** Speed and numerical stability of the various methods: propagation of the ground state in a harmonic oscillator potential over 4000 CM time steps of 2.5 fs. The user CPU time (CPU) is measured on a SUN Sparc 10. The values of $N_P$, $N_{QM}$ and $N_{exp}$ were reselected from all combinations given in Table 4 such that the standard deviation of the kinetic energy $\sigma(E_{kin})$ from the average times the user CPU time is minimal for each method. The rankings are derived from the product of the user CPU time and the standard deviation of the kinetic energy from the average. Otherwise as in Table 6

| *Method* | *ranking* | $N_P$ | $N_{QM}/N_{exp}$ | CPU[s] | $E_{kin}$[kJ/mol] | $\sigma(E_{kin})[10^{-4}$kJ/mol] |
|---|---|---|---|---|---|---|
| KRC | 5 | 16 | 64/– | 50.0 | 9.9754101 | 3.378 |
| KRC_S | 6 | 16 | $2^6$/– | 4.2 | 9.9796748 | 41.905 |
| KRSO | 7 | 16 | 256/– | 191.4 | 9.9757295 | 1.091 |
| KRSO_S | 4 | 32 | $2^6$/– | 2.3 | 9.9753923 | 7.781 |
| CKRSO | 9 | 16 | 128/– | 586.3 | 9.9746337 | 6.741 |
| DAF | 8 | 32 | 800/150 | 5144.9 | 9.9757727 | 0.046 |
| CH | 2 | 16 | 1/150 | 130.1 | 9.9757749 | 0.060 |
| SOD | 10 | 16 | 16384/– | 12282.4 | 9.9757761 | 3.382 |
| EE | 1 | 16 | 1/– | 27.8 | 9.9757774 | 0.007 |
| RES | 3 | 32 | 128/5 | 1092.9 | 9.9757773 | 0.011 |

**Table 9** Ranking of the integration schemes in terms of a minimum standard deviation of the kinetic energy from the average for different potentials and initial states. The first number is derived from 40 CM simulation steps, the second number is derived from 4000 CM simulation steps. Completely wrong results are indicated by *

| | *harmonic oscillator* | | | *double well potential* |
|---|---|---|---|---|
| *Method* | *ground state* | *1st excited* | *10th excited state* | *ground state* |
| KRC | 4/6 | 6/6 | 5/5 | –/4 |
| KRC_S | 6/10 | 8/9 | 8/8 | –/9 |
| KRSO | 5/5 | 5/5 | 4/4 | –/5 |
| KRSO_S | 7/9 | 9/8 | 7/6 | –/8 |
| CKRSO | 3/8 | 7/10 | 9/* | –/* |
| DAF | 2/4 | 4/4 | 6/3 | –/7 |
| CH | 1/3 | 1/3 | 1/2 | –/3 |
| SOD | 8/7 | 10/7 | 10/7 | –/6 |
| EE | 1/1 | 2/1 | 2/1 | –/1 |
| RES | 1/2 | 3/2 | 3/* | –/2 |

**Table 10** Ranking of the integration schemes in terms of a minimum standard deviation of the kinetic energy from the average times the user CPU time on a SUN Sparc 10 for different potentials and initial states. The first number is derived from 40 CM simulation steps, the second number is derived from 4000 CM simulation steps. Completely wrong results are indicated by *

| | *harmonic oscillator* | | | *double well potential* |
|---|---|---|---|---|
| *Method* | *ground state* | *1st excited* | *10th excited state* | *ground state* |
| KRC | 3/5 | 5/5 | 7/6 | –/4 |
| KRC_S | 7/6 | 4/8 | 6/5 | –/7 |
| KRSO | 6/7 | 7/6 | 5/4 | –/5 |
| KRSO_S | 8/4 | 6/4 | 4/3 | –/6 |
| CKRSO | 5/9 | 9/9 | 9/* | –/* |
| DAF | 9/8 | 8/7 | 8/7 | –/8 |
| CH | 2/2 | 2/2 | 2/2 | –/2 |
| SOD | 10/10 | 10/10 | 10/8 | –/9 |
| EE | 1/1 | 1/1 | 1/1 | –/1 |
| RES | 4/3 | 3/3 | 3/* | –/3 |



the average position and thus the kinetic and potential energy oscillate according to Ehrenfest's theorem, the standard deviation of the kinetic energy is not a suitable test for the accuracy and stability of an integration method in this case. Instead, the kinetic and potential energy trajectory and the elongation trajectory have been transformed from the time to the frequency domain using a discreate Fourier transform. The absolute value of the transform at frequency zero is then the average, and since the period of 10 fs is a multiple of the time step 2.5 fs, the amplitude of the observable can be read immediately from some points in the Fourier transform. The values which do not belong to either the frequency zero or the frequency 1/10 fs should vanish if a harmonic oscillator potential of this frequency is used. The sum over the absolutes of these

**Table 11** Propagation of a coherent state of a harmonic oscillator potential with mass 1.008 and period 10 fs over 4000 CM time steps of 2.5 fs. The amplitude of the initial state is 0.001 nm. Expected values are: Average of the kinetic energy: 10.07527 kJ/mol, harmonic part: 0.099485 kJ/mol, anharmonic part: 0 kJ/mol; average of the elongation: 0 nm, harmonic part: 0.001 nm, anharmonic part: 0 nm. The rankings are derived from the user CPU time (CPU) on a Sun Sparc 10 times the anharmonic part of the kinetic energy

| *Method* | *ranking* | *CPU* | *elongation* [$10^{-3}$nm] | | | *kinetic energy* [kJ/mol] | | |
|---|---|---|---|---|---|---|---|---|
| | | | *average* | *harmonic* | *anharm.* | *average* | *harmonic* | *anharm.* [$10^{-4}$] |
| KRC | 8 | 191.2 | 0.0000 | 1.0000 | 0.0000 | 10.0752595 | 0.0993441 | 0.010 |
| KRC_S | 7 | 4.0 | 0.0000 | 0.9998 | 0.0001 | 10.0741796 | 0.0997624 | 0.206 |
| KRSO | 6 | 49.9 | 0.0000 | 1.0000 | 0.0001 | 10.0745540 | 0.1001110 | 0.009 |
| KRSO_S | 5 | 1.1 | 0.0000 | 0.9999 | 0.0001 | 10.0669921 | 0.1001192 | 0.340 |
| CKRSO | 9 | 583.8 | 0.0000 | 0.9999 | 0.0000 | 10.0749306 | 0.0994960 | 0.014 |
| DAF | 4 | 3293.0 | 0.0000 | 1.0000 | 0.0000 | 10.0752512 | 0.0994973 | 0.000 |
| CH | 2 | 104.2 | 0.0000 | 1.0000 | 0.0000 | 10.0752629 | 0.0994894 | 0.000 |
| SOD | 10 | 3072.2 | 0.0000 | 1.0000 | 0.0000 | 10.0752628 | 0.0994847 | 0.018 |
| EE | 1 | 37.5 | 0.0000 | 1.0000 | 0.0000 | 10.0752629 | 0.0994855 | 0.000 |
| RES | 3 | 254.1 | 0.0000 | 1.0000 | 0.0000 | 10.0752620 | 0.0994835 | 0.000 |



remaining values is therefore called "anharmonic parts" in this table. Again, the eigenfunction expansion method is the fastest and most accurate integration scheme for the propagation in one dimension.

## CONCLUSIONS

The eigenfunction expansion method (EE) seems to be the most suitable integration scheme for the time-dependent Schrödinger equation of a one-dimensional quantum mechanical particle embedded in a classical mechanical chemical system. Besides, all considered methods except the corrected kinetic referenced split operator (CKRSO) method seem to be reasonably stable and accurate. From a comparison between the different simulations, it is clear that there is no "method of choice" which can be applied blindly. The distributed approximating functions (DAF) method produces very stable trajectories requiring considerable amounts of CPU time, while the Chebysheff series expansion (CH) is very accurate and fast. As it scales as $N_p \ln N_p$ with the number of grid points in the position representation, it is probably the best choice when going to more dimensions. In this case, the residuum minimization method (RES) might be very interesting as well since no special numerical problems have been found, and only the physically accessible range of the energy levels is considered. DAF, CH and RES need a very careful adjustment of their parameters, otherwise absolutely wrong results can be obtained even after a few steps. Both kinetic referenced split operator (KRSO) and Cayley (KRC) techniques are very easy to deal with, as long as the integration step is chosen small enough. These methods loose most of their stability when their performance is improved by matrix multiplication (KRSO_S and KRC_S). Since these two methods are by far the fastest methods if only a few grid points are required, they may become interesting as soon as there are methods to keep some quantities artificially

constant like kinetic energy and norm using coupling methods as is done routinely in classical MD simulations to keep the temperature and pressure constant [23]. Finally, the second order differencing scheme (SOD) which is a very easy scheme without any special parameters to adjust, requires too much CPU resources to obtain a reasonable accuracy.

Another important conclusion is that due to the relatively few grid points which are required for the considered problems, the use of one dimension allows the application of integrators which are more accurate and stable at even less computational expense (EE) than the integrators constructed to scale as slowly as possible with the size of the basis of the representation. Further work will be done on the EE, CH, RES, KRC and KRSO methods in one and three dimensions coupled to a classical subsystem with different techniques to solve the problems arising from time-dependent Hamiltonians, and the results shall be compared to time-dependent properties that are derived from imaginary-time path integral simulations. Finally, it should not be forgotten that solving the Schrödinger equation is only one (but important) part of non-relativistic quantum mechanics: correlations, symmetry, correspondence principle etc. have to be considered too.



## *References*


[1] P. Bala, B. Lesyng, T. N. Truong and J. A. McCammon, "Ab initio studies and quantum-classical molecular dynamics simulations for proton transfer processes in model systems and in enzymes", in *Molecular Aspects of Biotechnology: Computational Models and Theories*, J. Bertrán, ed, Kluwer, Dordrecht, 1992, pp. 299–326.

[2] C. Zheng, J. A. McCammon and P. G. Wolynes, "Quantum simulation of nuclear rearrangement in electron transfer reactions", *Proc. Natl. Acad. Sci. USA*, **86**, 6441 (1989).

[3] C. Zheng, J. A. McCammon and P. G. Wolynes, "Quantum simulations of conformation reorganization in the electron transfer reaction of tuna cytochrome c", *Chem. Phys.* **158**, 261 (1991)

[4] M. Marchi and D. Chandler, "Path-integral calculation of the tunnel splitting in aqueous ferrous-ferric electron transfer", *J. Chem. Phys.*, **95**, 889 (1991)

[5] H. Tal-Ezer, R. Kosloff and C. Cerjan, "Low-Order Polynomial Approximation of Propagators for the Time-Dependent Schrödinger Equation", *J. Comp. Phys.*, **100**, 179 (1992).

[6] U. Peskin, R. Kosloff, N. Moiseyev, "The solution of the time dependent Schrödinger equation by the $(t, t')$ method: The use of global polynomial propagators for time dependent Hamiltonians", *J. Chem. Phys.*, **100**, 8849 (1994).

[7] G. Yao, R. E. Wyatt, "Stationary approaches for solving the Schrödinger equation with time-dependent Hamiltonians", *J. Chem. Phys.*, **101**, 1904 (1994).

[8] U. Peskin, N. Moiseyev, "The solution of the time-dependent Schrödinger equation by the $(t, t)$ method: Theory, computational algorithm and applications", *J. Chem. Phys.*, **99**, 4590 (1993).

[9] P. Bala, B. Lesyng, J. A. McCammon, "Extended Hellmann-Feynman theorem for non-stationary states and its application in quantum-classical molecular dynamics simulations", *Chem. Phy. Lett.*, **219**, 259 (1994).

[10] R. Kosloff, "Time-Dependent Quantum-Mechanical Methods for Molecular Dynamics", *J. Phys. Chem.*, **92**, 2087 (1988).

[11] T. Iitaka, "Solving the time-dependent Schrödinger equation numerically", *Phys. Rev. E* **49**, 49 (1993).

[12] C. Leforestier, R. H. Bisseling, C. Cerian, M. D. Feit, R. Friesner, A. Guldberg, A. Hammerich, G. Jolicard, W. Karrlein, H. -D. Meyer, N. Lipkin, O. Roncero, and R. Kosloff, "A Comparison of different Propagation Schemes for the Time Dependent Schrödinger Equation", *J. comput. Phys.*, **94**, 59 (1991).

[13] N. Makri, "Feynman Path Integration in quantum dynamics", *Comp. Phys. Comm.*, **63**, 389 (1991).

[14] D. K. Hoffman. H. Nayar, O. A. Sharaffedin and D. J. Kouri, "Analytic Banded Approximation for the Discretized Free Propagator", *J. Phys. Chem.*, **95**, 8299 (1991).

[15] D. J. Kouri, W. Zhu, Xin Ma, B. M. Pettitt and K. K. Hoffman, "Monte Carlo Evaluation of Real-Time Feynman Path Integrals for Quantal Many- Body Dynamics: Distributed Approximating Function and Gaussian Sampling", *J. Phys. Chem.*, **96**, 9622 (1992).
[16] D. J. Kouri and D. K. Hoffman, "Toward a New Time-Dependent Path Integral Formalism Based on Restricted Quantum Propagators for Physically Realizable Systems", *J. Phys. Chem.*, **96**, 9631 (1992).
[17] N. Nayar, D. K. Hoffman, X. Ma and D. J. Kouri, "A Computational Demonstration of the Distributed Approximating Function Approach to Real time Quantum Dynamics", *J. Phys. Chem.*, **96**, 9637 (1992).
[18] T. J. Park, J. C. Light, "Unitary quantum time evolution by iterative Lanczos reduction", *J. Chem. Phys.*, **85**, 5870 (1986).
[19] B. P. Flannery, S. A. Teukolsky, W. T. Vetterling and W. H. Press, *Numerical Recipes in C, second edition*, Cambridge University Press, Cambridge USA, 1992, pp. 469–481.
[20] R. Kosloff, "Propagation methods for quantum molecular-dynamics", *Ann. Rev. Phys. Chem.*, **45**, 145 (1994).
[21] D. Makarov, N. Makri, "Path integrals for dissipative systems by tensor multiplication. Condensed phase quantum dynamics for arbitrarily long time", *Chem. Phys. Lett.*, **221**, 482 (1994).
[22] N. Makri, "Improved Feynman propagators on a grid and non-adiabatic corrections within the path integral framework", *Chem. Phys. Lett.*, **193**, 435 (1991).
[23] W. F. van Gunsteren and H. J. C. Berendsen, "Computer Simulation of Molecular Dynamics: Methodology, Applications, and Perspectives in Chemistry", *Angew. Chem. Int. Ed. Engl.*, **29**, 992 (1990).